

Article

Model Evaluation of the Microbial Metabolic Processes in a Hydrogen-Based Membrane Biofilm Reactor for Simultaneous Bromate and Nitrate Reduction

Minmin Jiang^{1,2}, Yuanyuan Zhang², Jie Zhang^{2,3,4}, Xingru Dai², Haixiang Li^{1,*}, Xuehong Zhang^{1,2}, Zhichao Wu⁴ and Junjian Zheng^{2,4,*} 

¹ Guangxi Key Laboratory of Environmental Pollution Control Theory and Technology, Guilin University of Technology, 319 Yanshan Street, Guilin 541006, China

² College of Life and Environmental Science, Guilin University of Electronic Technology, 1 Jinji Road, Guilin 541004, China

³ School of Chemistry and Materials Engineering, Huizhou University, 46 Yanda Road, Huizhou 516007, China

⁴ State Key Laboratory of Pollution Control and Resource Reuse, School of Environmental Science and Engineering, Tongji University, 1239 Siping Road, Shanghai 200092, China

* Correspondence: 2011042@glut.edu.cn (H.L.); zhengjunjianglut@163.com (J.Z.)

Abstract: The H₂-based membrane biofilm reactor (H₂-MBfR) has been acknowledged as a cost-effective microbial reduction technology for oxyanion removal from drinking water sources, but it remains unknown how the evolution of biofilm characteristics responds to the changing critical operating parameters of the H₂-MBfR for simultaneous bromate (BrO₃⁻) and nitrate (NO₃⁻) elimination. Therefore, an expanded multispecies model, applicable to mechanistically interpret the bromate-reducing bacteria (BRB)- and denitrifying bacteria (DNB)-dominated metabolic processes in the biofilm of the H₂-MBfR, was developed in this study. The model outputs indicate that (1) increased BrO₃⁻ loading facilitated the metabolism of BRB by increasing BRB fraction and BrO₃⁻ gradients in the biofilm, but had a marginal influence on NO₃⁻ reduction; (2) H₂ pressure of 0.04 MPa enabled the minimal loss of H₂ and the extension of the active region of BRB and DNB in the biofilm; (3) once the influent NO₃⁻ concentration was beyond 10 mg N/L, the fraction and activity of BRB significantly declined; (4) BRB was more tolerant than DNB for the acidic aquatic environment incurred by the CO₂ pressure over 0.02 MPa. The results corroborate that the degree of microbial competition for substrates and space in the biofilm was dependent on system operating parameters.

Keywords: BrO₃⁻; NO₃⁻; bioreactor; microbial reduction; multispecies model; biofilm characteristics



Citation: Jiang, M.; Zhang, Y.; Zhang, J.; Dai, X.; Li, H.; Zhang, X.; Wu, Z.; Zheng, J. Model Evaluation of the Microbial Metabolic Processes in a Hydrogen-Based Membrane Biofilm Reactor for Simultaneous Bromate and Nitrate Reduction. *Membranes* **2022**, *12*, 774. <https://doi.org/10.3390/membranes12080774>

Academic Editor: José M. Gozálviz-Zafrilla

Received: 19 July 2022

Accepted: 10 August 2022

Published: 11 August 2022

Publisher's Note: MDPI stays neutral with regard to jurisdictional claims in published maps and institutional affiliations.



Copyright: © 2022 by the authors. Licensee MDPI, Basel, Switzerland. This article is an open access article distributed under the terms and conditions of the Creative Commons Attribution (CC BY) license (<https://creativecommons.org/licenses/by/4.0/>).

1. Introduction

Bromate (BrO₃⁻), a common disinfection byproduct formed during the advanced oxidation processes (especially ozonation) of drinking water, has been assigned as a Group 2B carcinogen with a maximum contaminant level of 10 µg/L in potable water by the World Health Organization [1–3]. The BrO₃⁻ concentration varies typically from below 30 µg/L in the ozonated surface water to 0.8–1.4 mg/L in the groundwater intruded by industrial discharges [2,4]. Current physicochemical approaches for aquatic BrO₃⁻ elimination, involving adsorption, separation, chemical reduction, and photo-/electro-catalysis, exhibit limited application potential due to their disadvantages in terms of high energy consumption, stringent optional conditions, and requirements of post-treatment steps [5–7]. Comparably, autotrophic microbial reduction has received increasing interest in the past decade, owing to its proven capacity of cost-efficiently converting BrO₃⁻ to innocuous Br⁻ under mild circumstances and the organic-deficient nature of most drinking water sources [6,8].

Nitrate (NO₃⁻) is a pervasive contaminant which coexists with BrO₃⁻ at a typical concentration range of 10–30 mg N/L in surface water and groundwater, and which can

result in methemoglobinemia in infants [8–11]. This accentuates the necessity to develop robust technology capable of simultaneously eliminating BrO_3^- and NO_3^- from polluted drinking water sources. As an advanced autotrophic microbial reduction technology, the H_2 -based membrane biofilm reactor (H_2 -MBfR) has been successfully practiced at a pilot and/or commercial scale for eradicating a variety of oxidized pollutants, e.g., BrO_3^- , NO_3^- , sulfate, perchlorate, selenate, and chromate [9,12]. In this system, electron donor H_2 diffuses through the wall of gas-permeable hollow fiber membranes (HFM), and supports the functional microorganisms in the HFM-attached biofilm to respire the electron acceptors (i.e., oxidized pollutants); such a scheme of passive gas delivery enables the full utilization of H_2 , as well as the efficient removal of targeted contaminants [9,13]. Several case studies have shown that, when the influent concentrations of BrO_3^- and NO_3^- were in the range of 0.1–1.5 mg/L and 5–20 mg N/L, respectively, which were approachable to those in real drinking water sources, the appreciable removal (beyond 95%) of both oxyanions could be realized in H_2 -MBfRs [1,8].

In H_2 -MBfRs, the biofilm microorganisms, which can dominate the reduction of BrO_3^- and NO_3^- , are defined as bromate-reducing bacteria (BRB) and denitrifying bacteria (DNB), respectively [1,11]. Since H_2 is shared by functional bacteria (e.g., BRB and DNB) in the biofilm as the sole electron donor to drive the reduction of oxidized pollutants, the microbial competition for H_2 availability (controlled by H_2 supplying pressure) inevitably occurs in H_2 -MBfRs [14]. The results of empirical studies corroborated that BrO_3^- and NO_3^- concentrations were critical to the efficiencies of microbial reduction, and the BrO_3^- reduction processes could be inhibited in the case of exorbitant NO_3^- loading [11,15]. Microbial community investigations have revealed the variation trends in the species and abundance of BRB and DNB in the biofilm systems under diverse BrO_3^- and NO_3^- loadings [6,11]. Despite the above progress, it remains understudied the extent to which the critical operating parameters drive the evolution of biofilm microenvironment, structure, and activity of the H_2 -MBfR for simultaneous BrO_3^- and NO_3^- elimination. This constitutes a major hindrance to our understanding of the interaction mechanism between BRB and DNB in the biofilm. The development of a systematic and quantitative framework might be a solution to this concern, given the difficulty in the use of present experimental means for elucidating the stratification features of biofilm.

The one-dimensional, multispecies biofilm model, developed on the AQUASIM platform, is a versatile tool applicable to quantitatively assess the steady-state characteristics of the biofilm, e.g., the substrate profiles, as well as microbial distribution and activities [16]. To date, a model framework, which can be implemented to simulate the simultaneous removal processes of BrO_3^- and NO_3^- in the H_2 -MBfR, is still unavailable in the literature. In this work, a sophisticated biofilm model was established on the AQUASIM platform to mechanistically interpret the BrO_3^- and NO_3^- reduction processes of H_2 -MBfR. On the basis of the previous model frameworks for NO_3^- removal [14,16], we proposed an expanded model framework through incorporation into the algorithm for the metabolic process kinetics of BRB, as well as the influences of CO_2 addition (as carbon source and pH regulator) on metabolic process kinetics of BRB and DNB. Long- and short-term experimental data regarding BrO_3^- and NO_3^- removal, obtained from a lab-scale H_2 -MBfR, were used for the calibration of key model parameters and the validation of the model outputs, respectively. The validated model was then applied to evaluate the gradients of substrates (H_2 , BrO_3^- , and NO_3^-), as well as the distribution and activities of BRB and DNB in the biofilm, in the case of changing system operating parameters including the H_2 pressure, CO_2 addition, and influent BrO_3^- and NO_3^- concentrations.

2. Materials and Methods

2.1. Reactor Setup and Start-Up

The schematic of the H_2 -MBfR used in this study is shown in Figure 1. The reactor consisted of a module containing 96 HFMs (Litree Company, Suzhou, China) and a microporous tube placed in a plexiglass cylinder (height = 22 cm, inner diameter = 6 cm,

effective volume = 0.56 L). The average outer diameter and pore size of HFM was 1.5 mm and 0.02 μm , respectively, and the total membrane surface area of HFM module was 633 cm^2 . The module with a sealed lower end was connected to a H_2 tank for delivering pressurized H_2 . Pure CO_2 was supplied by the microporous tube with its bottom end linked to a CO_2 tank to serve as carbon source and pH regulator. Synthetic influent was introduced into the reactor via a peristaltic pump (BT101L-DG-1, Lead Fluid, Baoding, China), and the effluent was collected from the outlet of the reactor. A recirculation pump (BT101L-YZ15/25, Lead Fluid, Baoding, China) was sustained at a high flowrate of 100 mL/min to keep the bulk liquid completely mixed. The reactor was inoculated with 50 mL of biomass collected from a denitrifying H_2 -MBfR in our lab. The synthetic influent, containing 10 mg N/L NaNO_3 with an identical composition to that described in Li et al. [17], was used in the start-up period of the reactor. During the start-up period, the influent flowrate was maintained at 1.6 mL/min (resulting in an HRT of 5.8 h), and the H_2 and CO_2 pressure was kept at 0.04 and 0.012 MPa, respectively. After 30 days of operation, the influent flowrate was changed to 2.0 mL/min (corresponding to an HRT of 4.7 h) until the biofilm was well formed, and the performance of the reactor reached a steady state with stable NO_3^- removal.

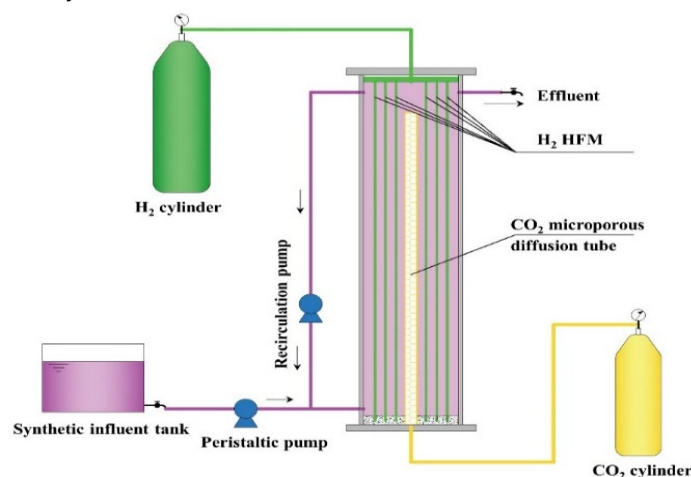


Figure 1. Schematic of the H_2 -MBfR.

2.2. Short- and Long-Term Experiments and Sample Analysis

On days 31–40 of stage 1, short-term experiments were performed to assess the effects of H_2 pressure (0.01–0.08 MPa), influent NO_3^- (1–20 mg N/L), and CO_2 pressure (0.004–0.036 MPa) on the NO_3^- and BrO_3^- removal of the H_2 -MBfR. The detailed information concerning the operational conditions of short-term experiments can be found in Table S1. For each experiment, one system operating parameter was changed, while keeping the others fixed. Once the experiment condition was changed, aqueous samples were collected after three HRT operations of the system, in order to allow the stabilization of effluent contaminant concentrations [18]. Following the short-term experiments, long-term experiments (days 41–140) were carried out to investigate how the oxyanion removal performance of the system responded to the changing BrO_3^- loadings. As summarized in Table S2, in long-term experiments, the influent concentrations of BrO_3^- were set at 0.1, 0.5, and 1.0 mg/L in stage 3, stage 4, and stage 5, respectively, and the H_2 and CO_2 pressure were maintained at 0.04 and 0.012 MPa, respectively.

The collected aqueous samples were filtered immediately through a 0.22 μm pore size polycarbonate membrane filter (Anpel Co., Ltd., Shanghai, China) and stocked in a refrigerator (4 $^\circ\text{C}$) until analyzed. The concentrations of NO_3^- , NO_2^- , and BrO_3^- were determined by ion chromatography (ICS-1000, Dionex, Sunnyvale, USA) equipped with an AS-19 column (4 \times 250 mm, Dionex, Sunnyvale, USA). The dissolved H_2 was determined using a H_2 microsensor (H_2 10, Unisense A/S Corp., Aarhus, Denmark). The pH value was

measured using a pH meter (pHS-3C model, Leici, Shanghai, China). The contaminant removal flux was calculated using Equation (1):

$$J = \frac{Q}{A}(S_i - S_e), \tag{1}$$

where J is the NO_3^- and BrO_3^- removal flux in units of $\text{g N}/(\text{m}^2 \cdot \text{day})$ and $\text{g BrO}_3^- /(\text{m}^2 \cdot \text{day})$, respectively, Q signifies the influent flowrate (m^3/day), A refers to the total membrane surface area (m^2), and S_i and S_e denote the influent concentration of NO_3^- or BrO_3^- and the effluent concentration of NO_3^- or BrO_3^- , respectively.

2.3. Model Development and Evaluation

2.3.1. Model Framework Development

Unlike the classical biofilm models established by Tang et al. [14,16], the framework of the developed mathematical model involves the biochemical process of hydrogenotrophic BrO_3^- reduction, and it considers the effects on the metabolic process kinetics of BRB and DNB in the case of CO_2 addition (as carbon source and pH regulator). Figure 2 shows the schematic of the involved biochemical processes and the correlated interactions between the model components in the biofilm. The model components include five solid components (i.e., BRB, DNB, heterotrophic bacteria (HB), extracellular polymeric substances (EPS), and inert organics (IO)) and five dissolved components (i.e., H_2 , CO_2 , NO_3^- , BrO_3^- , and soluble microbial products (SMP)). H_2 is exploited by BRB and DNB as the electron donors, BrO_3^- and NO_3^- as the electron acceptors, and CO_2 as the carbon source. In the conversion processes of BrO_3^- and NO_3^- to Br^- and N_2 , BRB and DNB obtain energy to sustain their growth and metabolism. H_2 was the sole energy source of the hydrogenotrophic bacteria, since no organic carbon was introduced to the influent; thus, BRB and DNB could merely abstract electrons from H_2 to drive the BrO_3^- and NO_3^- reduction. HB grows either on the SMP directly produced by BRB and DNB or indirectly on the hydrolyzed EPS (i.e., SMP) originated from BRB and DNB. The decay of BRB, DNB, and HB generates nonbiodegradable IO. The electrons provided from H_2 can be classified into three portions during the BRB and DNB metabolic processes: bacterial cell synthesis (k_1), SMP formation (k_2), and EPS formation (k_3); thus, $k_1 + k_2 + k_3 = 1$. The electrons for cell synthesis are subdivided into the fraction for energy-providing reaction (f_e^0) and the other for synthesis reaction of true yield of biomass (f_s^0); therefore, $f_e^0 + f_s^0 = 1$. Here, f_d represents the fraction of biodegradable biomass; hence, $1 - f_d$ refers to the remaining nonbiodegradable biomass.

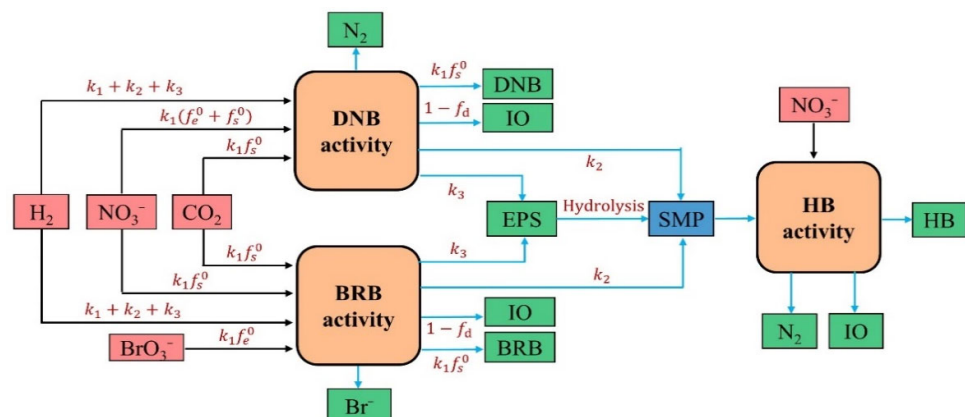


Figure 2. Schematic of the interactions between model components involved in the biochemical processes of the biofilm.

2.3.2. Model Solution and Calibration

The numerical solution of the model was implemented on software AQUASIM 2.1g, by inputting the process matrix (Table 1), stoichiometric and kinetic parameters (Table S3), process kinetic rate equations (Table 2), and experiment operational parameters of the

H₂-MBfR (Table S4). In particular, the calculation procedure for stoichiometric coefficients of model components (shown in Table 1) in the BRB metabolic process is exhibited in Section S1. Table S3 merely lists the calculated and recalibrated stoichiometric and kinetic parameters of the BRB metabolic process in this work, while other pertinent parameters can be found in Table S5. Bulk liquid pH is known to be a key factor correlated to the activities of the hydrogenotrophic microorganisms [13,19,20]. In order to quantitatively assess how bulk liquid pH affects the microbial metabolic activities, the inhibition factor of bulk liquid pH (f_{pH}) was introduced to the kinetic rate expressions of the model framework, as shown in Table 2. According to the normalized Michaelis pH function [21], f_{pH} can be computed using Equation (2).

$$f_{pH} = \frac{1 + 2 \cdot 10^{0.5(pK_l - pK_h)}}{1 + 10^{(pH - pK_h)} + 10^{(pK_l - pH)}} \quad (2)$$

where pH values are the experimental measurements in this study; pK_h and pK_l denote the upper and lower pH values at which the metabolic rates are equal to 50% of the maximum rate at the optimum pH, respectively, and their values of 9.04 and 6.27 were adopted from previous studies [21–23].

Table 1. Process matrix for the developed model of components.

Component (i) Process (j)	S _{H2}	S _{NO3}	S _{BrO3}	S _{SMP}	S _{CO2}	X _{DNB}	X _{BRB}	X _{HB}	X _{IO}	X _{EPS}
DNB growth	$-\frac{14}{5f_{s,DNB}^0}$	$-k_1 \left(\frac{28f_{e,DNB}^0}{25f_{s,DNB}^0} + \frac{1}{5} \right)$		k_2	$-k_1$	k_1				k_3
BRB growth	$-\frac{14}{5f_{s,BRB}^0}$	$-\frac{1}{5}k_1$	$-k_1 \frac{14f_{e,DNB}^0}{15f_{s,DNB}^0}$	k_2	$-k_1$		k_1			k_3
HB growth		$-\frac{1-Y_{HB}}{1.25Y_{HB}}$		$-\frac{1}{Y_{HB}}$				1		
DNB decay						-1				$1-f_d$
BRB decay							-1			$1-f_d$
HB Decay								-1		$1-f_d$
Hydrolysis				1						-1
	H ₂ (mol/m ³)	NO ₃ (mol/m ³)	BrO ₃ (mol/m ³)	SMP (mol/m ³)	CO ₂ (mol/m ³)	DNB (mol/m ³)	BRB (mol/m ³)	HB (mol/m ³)	IO (mol/m ³)	EPS (mol/m ³)

Table 2. Process kinetic rate equations for the developed model.

Process (j)	Kinetic Rate Expressions
DNB growth	$\mu_{DNB} \frac{S_{H_2}}{S_{H_2} + K_{H_2}^{DNB}} \frac{S_{NO_3}}{S_{NO_3} + K_{NO_3}^{DNB}} \frac{S_{CO_2}}{S_{CO_2} + K_{CO_2}^{DNB}} X_{DNB} f_{pH}$
BRB growth	$\mu_{BRB} \frac{S_{H_2}}{S_{H_2} + K_{H_2}^{BRB}} \frac{S_{NO_3}}{S_{NO_3} + K_{NO_3}^{BRB}} \frac{S_{BrO_3}}{S_{BrO_3} + K_{BrO_3}^{BRB}} \frac{S_{CO_2}}{S_{CO_2} + K_{CO_2}^{BRB}} X_{BRB} f_{pH}$
HB growth	$\mu_{HB} \frac{S_{NO_3}}{S_{NO_3} + K_{NO_3}^{HB}} \frac{S_{SMP}}{S_{SMP} + K_{SMP}^{HB}} X_{HB} f_{pH}$
DNB decay	$b_{DNB} X_{DNB}$
BRB decay	$b_{BRB} X_{BRB}$
HB Decay	$b_{HB} X_{HB}$
Hydrolysis	$k_{hyd} X_{EPS}$

Disparate reactor configurations, operating conditions, and HFM patterns commonly result in the varying compositions and metabolic kinetics of biofilms [24]. For the aim of matching the specific simulation scenarios, several parameters, i.e., H₂ transfer coefficient of HFM (K_m), maximum specific growth rate of DNB and BRB (μ_{DNB} and μ_{BRB}), and half-maximum-rate concentration of BrO₃⁻ for BRB (K_{BrO_3}), were recalibrated by fitting the measured effluent NO₃⁻ and BrO₃⁻ concentrations of the long-term operated system to the modeled results using the AQUASIM built-in iterative algorithms (Equation (3)).

By minimizing the square error sums between the model predictions and experimental measurements, the selected parameters were calibrated to be the best-fit values.

$$\chi^2(p) = \sum_{i=1}^n \left(\frac{y_{meas,i} - y_i(p)}{\sigma_{meas,i}} \right)^2, \tag{3}$$

where $y_{meas,i}$ and $y_i(p)$ represent the experimental results and model predictions at time i , and $\sigma_{meas,i}$ and n signify the standard deviation and number of data points, respectively.

2.3.3. Model Validation and Evaluation

The calibrated model was further validated by comparing the simulated results with experimentally measured NO_3^- and BrO_3^- removal fluxes in the short-term experiments. The validated model was then used to simulate the profiles of substrates, microbial distribution, and metabolic activities in the biofilm of the H_2 -MBfR operated in a series of system conditions, including influent BrO_3^- concentrations (0.1–1.0 mg/L), H_2 pressure (0.01–0.08 MPa), influent NO_3^- concentration (1–20 mg N/L), and CO_2 pressure (0.004–0.036 MPa), in order to investigate the evolution laws of biofilm microenvironment, structure, and activity in the H_2 -MBfR for NO_3^- and BrO_3^- removal, in the case of changing system conditions. A schematic of the research methodology is shown in Figure 3.

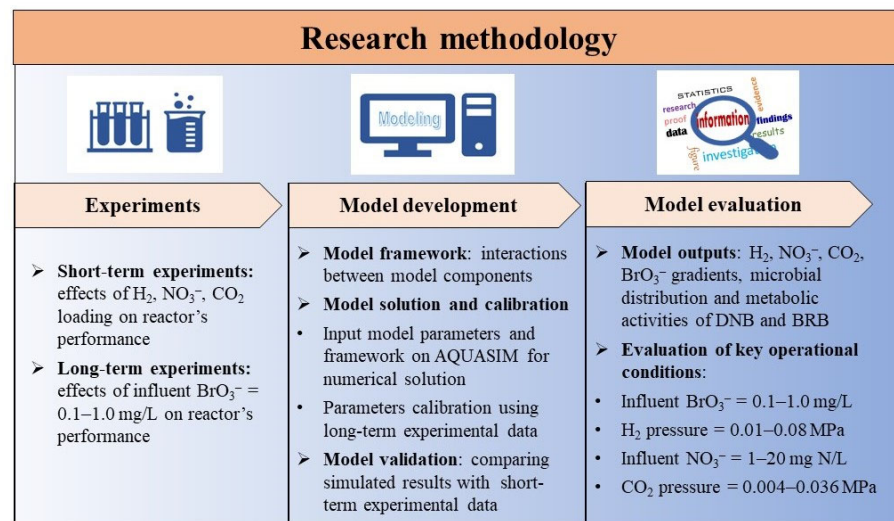


Figure 3. Schematic of the research methodology.

3. Results and Discussion

3.1. Long-Term H_2 -MBfR Performance and Model Calibration

The long-term experimental data obtained during the 140 days of operation of H_2 -MBfR were used for the recalibration of the selected parameters by fitting the effluent NO_3^- and BrO_3^- concentrations to those of simulated results. As shown in Figure 4, the measured data and simulated results were finely matched with the corresponding coefficients of determination (R^2) up to 0.93 and 0.91 for the effluent NO_3^- and BrO_3^- concentrations, respectively. The analysis results concerning the sensitivity of the selected parameters to the effluent BrO_3^- and NO_3^- concentrations in the long-term operated H_2 -MBfR are shown in Figure 5. It can be found that the effluent BrO_3^- concentration of the H_2 -MBfR was most sensitive to μ_{BRB} and relatively sensitive to μ_{DNB} and K_m (Figure 5a), while the effluent NO_3^- concentration was sensitive to K_m and μ_{DNB} (Figure 5b). These results are in line with the findings of previous studies, i.e., the maximum specific growth rate of microorganisms and the H_2 transfer coefficient of HFM were sensitive to the H_2 -MBfR performance [9,24,25]. The best-fit values of K_m , μ_{BRB} , μ_{DNB} , and K_{BrO_3} were estimated to be 0.189 m/day, 0.85 day^{-1} , 0.57 day^{-1} , and 0.014 mg/L , respectively.

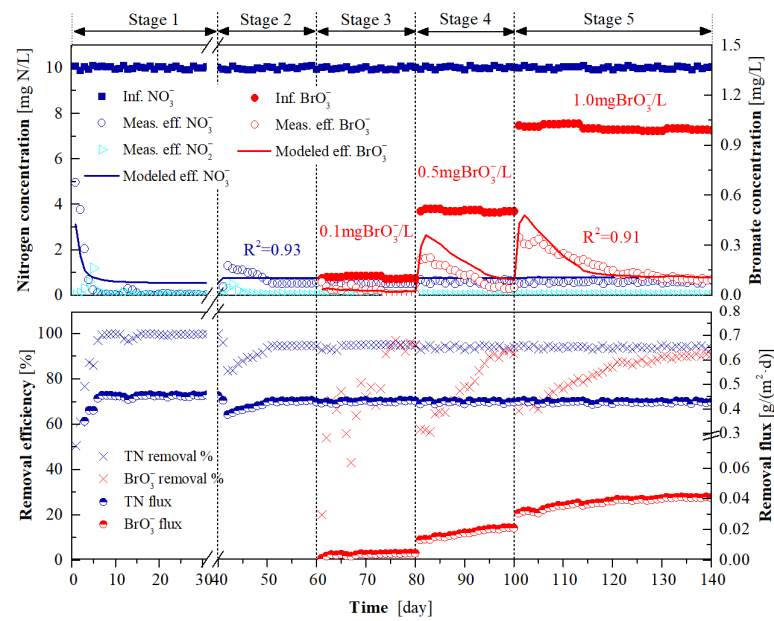


Figure 4. Long-term performance of NO_3^- and BrO_3^- reduction in the H_2 -MBfR. The abbreviations “Inf.,” “Eff.,” and “Meas.” denote influent, effluent, and measured, respectively.

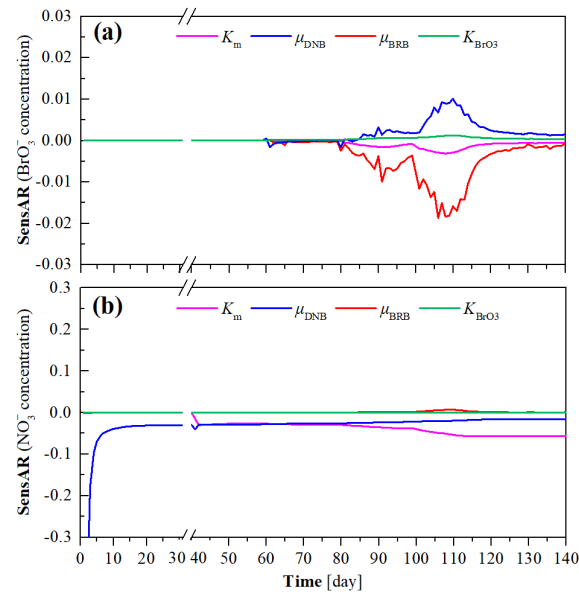


Figure 5. Sensitivities of the effluent BrO_3^- (a) and NO_3^- (b) concentrations to the selected parameters K_m , μ_{DNB} , μ_{BRB} , and K_{BrO_3} .

It can be also seen from Figure 4 that, after 7 days of start-up at stage 1, the denitrification flux of the H_2 -MBfR stabilized at around $0.45 \text{ g N}/(\text{m}^2 \cdot \text{day})$, corresponding to a NO_3^- removal efficiency of over 99%. The slightly decreased denitrification flux of the system at stage 2 can be ascribed to the augment in the influent flowrate from 1.6 mL/min at stage 1 to 2.0 mL/min at this stage. The introduction of 0.1–1.0 mg/L BrO_3^- into the influent at stages 3–5 did not further decrease the denitrification performance of the system, given the identical average denitrification flux ($0.42 \text{ g N}/(\text{m}^2 \cdot \text{day})$) at days 50–60 of stage 2 (without BrO_3^- addition) and stages 3–5. This observation is in agreement with the results of previous studies that a BrO_3^- concentration below 50 mg/L had no inhibitory effect on denitrification [15,26]. Empirical studies suggest that it usually takes 11–40 days to enable the H_2 -MBfRs to reach steady-state characteristics following the adjustment of operation conditions such as substrate loadings and HRT [17,27]. Similarly, our results

indicate that, in the case of BrO_3^- addition, it took 15–25 days at stages 3–5 to enable the BrO_3^- removal of the H_2 -MBfR to reach a steady state. The stabilized BrO_3^- removal flux was increased from $0.0044 \text{ g}/(\text{m}^2 \cdot \text{day})$ at stage 3 to $0.041 \text{ g}/(\text{m}^2 \cdot \text{day})$ at stage 5. This is presumably attributed to the augment in the abundance and/or reduction rate of BRB with increasing influent BrO_3^- concentration. Furthermore, Downing and Nerenberg [15] found that a near 11-fold increase in the BrO_3^- removal flux of H_2 -MBfR was achieved when the influent BrO_3^- concentration was increased from 0.1 to 10 mg/L.

3.2. Short-Term H_2 -MBfR Performance and Model Validation

Short-term experiments were performed to evaluate the effects of the key influencing factors, i.e., H_2 pressure, influent NO_3^- concentration, and CO_2 pressure, on the NO_3^- and BrO_3^- reduction of the H_2 -MBfR. As shown in Figure 6a,b the determined BrO_3^- and NO_3^- removal fluxes were increased from 0.036 and 0.36 to $0.041 \text{ g}/(\text{m}^2 \cdot \text{day})$ and $0.42 \text{ g N}/(\text{m}^2 \cdot \text{day})$, respectively, as the H_2 pressure was increased from 0.01 to 0.04 MPa. This is likely owing to the increased availability of electron donor, which enhanced the activities of BRB and DNB. A higher H_2 pressure (0.06 and 0.08 MPa) did not ameliorate the BrO_3^- and NO_3^- removal, but led to the consumption of the remaining H_2 in the effluent. Figure 6c,d delineate that, although the BrO_3^- and NO_3^- were all accumulated in the effluent, the NO_3^- removal flux was increased from 0.42 to $0.51 \text{ g N}/(\text{m}^2 \cdot \text{day})$, accompanied by the significant decrease in BrO_3^- removal flux from 0.041 to $0.011 \text{ g}/(\text{m}^2 \cdot \text{day})$, when the influent NO_3^- concentrations were augmented from 10 to 20 mg N/L. In accordance with this, Zhong et al. [6] observed that an influent NO_3^- concentration of 11.3 mg N/L was able to inhibit the BrO_3^- reduction in the H_2 -MBfR, which gave rise to the advantage of DNB over BRB when competing for electron donors. CO_2 is arguably one of the most effective pH regulators in H_2 -MBfRs, and it can serve as the supplemental inorganic carbon source for hydrogenotrophic bacteria [13,28]. As depicted in Figure 6e,f, the shift of CO_2 pressure from 0.012 to 0.036 MPa led to an apparent decline in the NO_3^- removal flux from $0.42 \text{ g N}/(\text{m}^2 \cdot \text{day})$ at 0.012 MPa to $0.32 \text{ g N}/(\text{m}^2 \cdot \text{day})$ at 0.036 MPa, but had a negligible influence on BrO_3^- removal flux. A plausible explanation is that, as the CO_2 pressure was in the range of 0.020–0.036 MPa, the resultant bulk liquid pH of 6.0–6.9 was obviously lower than the reported favorable pH range (7.0–9.0) of DNB, according to existing studies [19,20], and some specific BRB was possibly able to endure more acidic conditions. Additionally, the measured removal fluxes of BrO_3^- and NO_3^- in the short-term experiments were employed to further validate the calibrated model. It can be observed from Figure 6b–f that, in all cases, the modeled results were quite approximate to the experimental data, indicating the good accuracy and reliability of the developed model for prediction of the simultaneous BrO_3^- and NO_3^- reduction processes in the H_2 -MBfR.

3.3. Model Evaluation of the Effects of BrO_3^- Loading

Figure 7 shows the simulated distribution of substrates, DNB and BRB fractions, as well as their metabolic activities, in the steady-state biofilms at stages 3–5 using the validated model. As shown in Figure 7a–c, in line with the counter-diffusional characteristics of dissolved substrate in H_2 -MBfR biofilm [29], the H_2 concentration gradually decreased from HFM surface (i.e., biofilm thickness of zero point) toward to the bulk liquid side, while the other substrates (including CO_2 , NO_3^- , and BrO_3^-) originated from bulk liquid presented the contrary tendency. H_2 and CO_2 concentrations across the biofilm exhibited negligible difference when the influent concentration varied in the range of 0.1–1.0 mg/L (Figure 7a), attributed to the limited electron donor and carbon source consumption by BRB at low BrO_3^- loadings. It can also be seen from Figure 7a that CO_2 was not a limiting factor as a carbon source for BRB and DNB anabolism, since its concentrations within the whole biofilm were much higher than the half-maximum-rate concentration (0.004 mg/L) adopted in the model. Moreover, the resultant bulk liquid pH 7.5 at the CO_2 pressure of 0.012 MPa would not adversely affect the metabolic processes of BRB and DNB, since the maximum NO_3^- and BrO_3^- removal fluxes were attained at this CO_2 pressure, as shown

in Figure 6f. In line with this, the optimal pH reported for hydrogenotrophic denitrification and bromate reduction has been documented at neutral or weakly alkaline values [13,15].

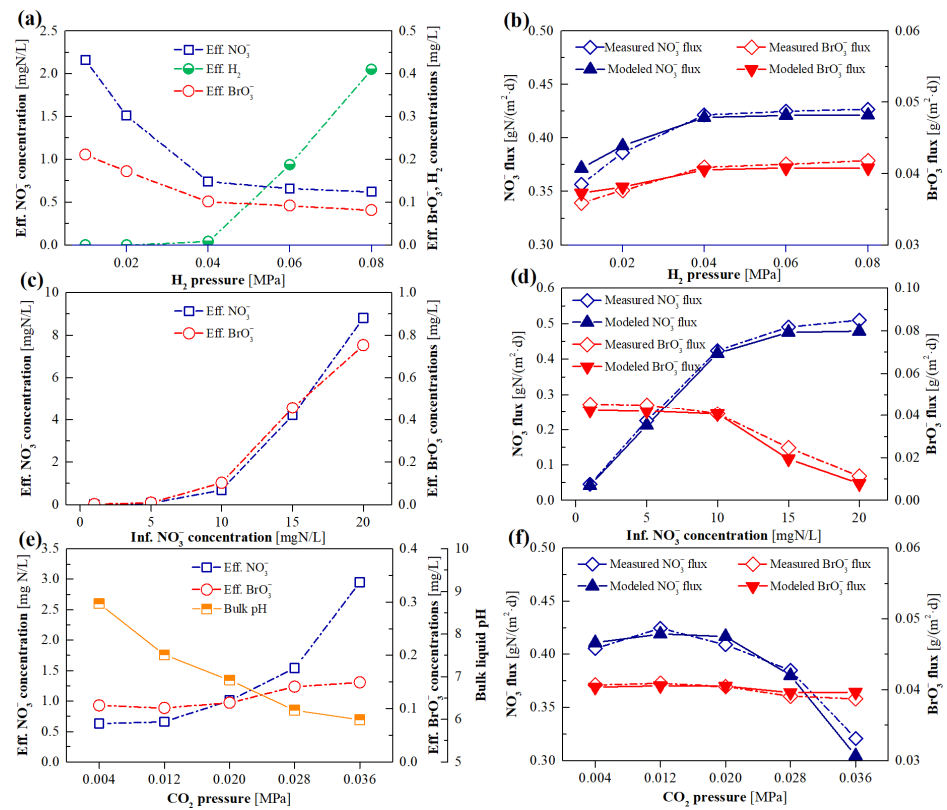


Figure 6. The system performance of the H_2 -MBfR, as well as the comparison of the measured and simulated removal fluxes of NO_3^- and BrO_3^- , in the case of changing H_2 pressure (a,b), influent NO_3^- concentration (c,d), and CO_2 pressure (e,f).

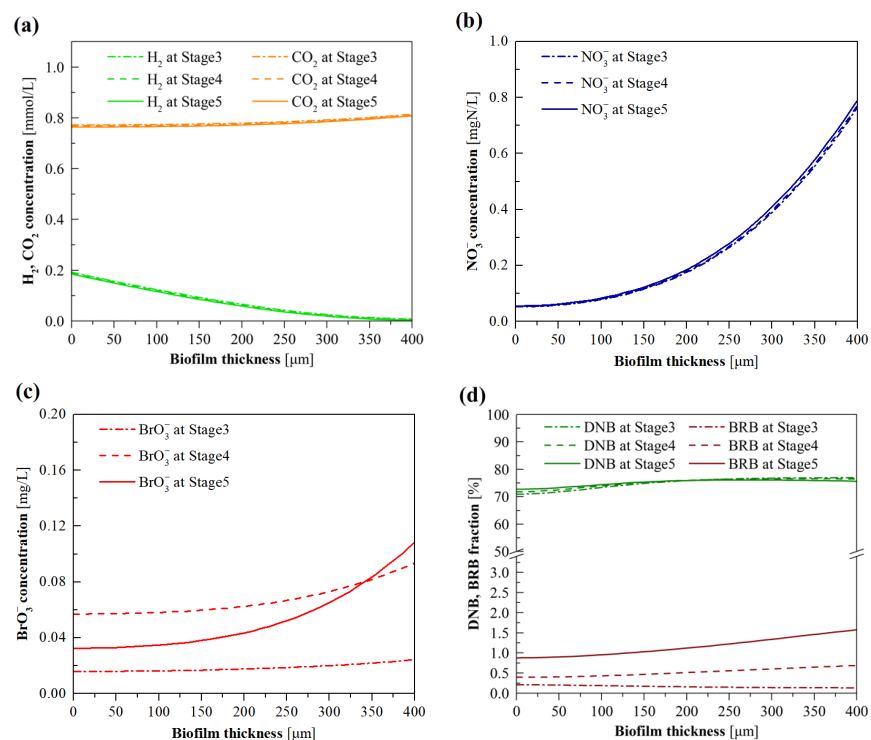


Figure 7. Cont.

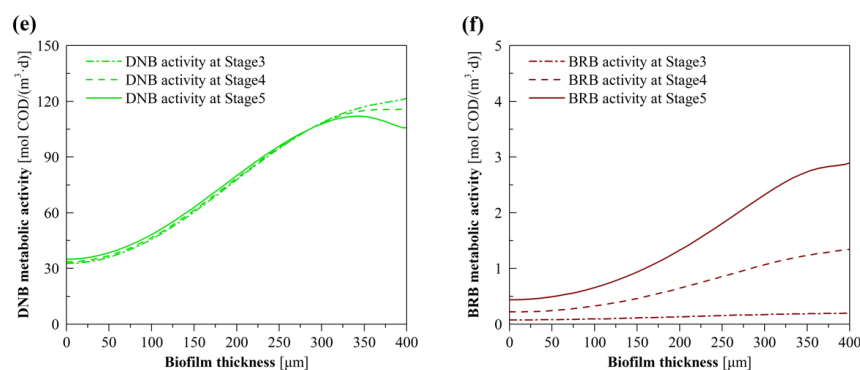


Figure 7. Model-simulated profiles for (a) H_2 and CO_2 , (b) NO_3^- , (c) BrO_3^- concentrations, and (d) DNB and BRB fractions, as well as (e) DNB and (f) BRB metabolic activities, in the biofilm of H_2 -MBfR as a function of influent BrO_3^- concentration ranging from 0.1 to 1.0 mg/L.

Figure 7d plots the simulated profiles of DNB and BRB fractions in the biofilm. DNB dominated in the biofilm compared to BRB at all stages, indicating that DNB outcompeted BRB for space, likely associated with the much higher concentration of NO_3^- in the biofilm than BrO_3^- . In particular, in response to the increase of the influent BrO_3^- concentration from stage 3 to stage 5, the BRB fraction (proportion) obviously increased in the biofilm. Figure 7e shows the DNB activity in the biofilm as a function of influent BrO_3^- concentration. The declined DNB activity in the biofilm range of 0–210 μm was mainly due to the inhibition of electron acceptors for DNB metabolism, given that the NO_3^- concentrations within this range were below the half-maximum-rate concentration of NO_3^- for DNB (0.2 mg N/L) [14]. The observed decrease in DNB activity from stage 3 to stage 5 at the outer layer biofilm was the result of the lower H_2 concentrations. As shown in Figure 7f, the BRB activity in the biofilm increased from stage 3 to stage 5, owing to the augmented BRB fraction and BrO_3^- gradients in the biofilm, which facilitated the metabolism of BRB. In addition, the increased BRB fraction and activity, as exhibited in Figure 7d,f, helps explain the augmented BrO_3^- removal flux from stage 3 to stage 5 (Figure 4).

3.4. Model Evaluation of the Effects of H_2 Pressure

Empirical studies [13,20] have collectively shown that excessive H_2 supply pressure results in the H_2 off-gassing problem, while an insufficient supply leads to unsatisfactory pollutant removal due to the electron donor scarcity in biofilms. Figure 8a plots the simulated H_2 and CO_2 concentration profiles in the biofilm at diverse H_2 pressure (0.01–0.08 MPa). The H_2 concentration in the biofilm increased with the increase in H_2 pressure. At the H_2 pressure of 0.01 MPa, more than half of the outer biofilm region (biofilm thickness > 200 μm) could not deliver sufficient H_2 . H_2 constitutes a limiting factor for microbial metabolic processes when its content is below the half-maximum-rate concentration. When H_2 pressure was increased to 0.04 MPa, the H_2 contents across the biofilm were all higher than the half-maximum-rate concentrations of H_2 for DNB and BRB metabolism (0.002 mg/L) [14]; thus, it can be inferred that the H_2 concentration within biofilm was not a decisive factor limiting NO_3^- and BrO_3^- removal at relatively high H_2 pressure. Note that, at this H_2 pressure, the simulated H_2 concentration in the bulk liquid was 0.0074 mg/L, which is quite close to the measured result (0.008 mg/L) during the short-term experiments (Figure 6a) and is also comparable to the recommended aquatic H_2 concentration (0.009 mg/L) in H_2 -MBfR [18]. Upon further increasing the H_2 pressure, the H_2 off-gassing phenomenon occurred. It can also be seen from Figure 8a that the CO_2 concentration gradients in the biofilm hardly changed when the H_2 pressure was higher than 0.04 MPa. This implies that the excessive H_2 supply would not accelerate the carbon source utilization of BRB and DNB.

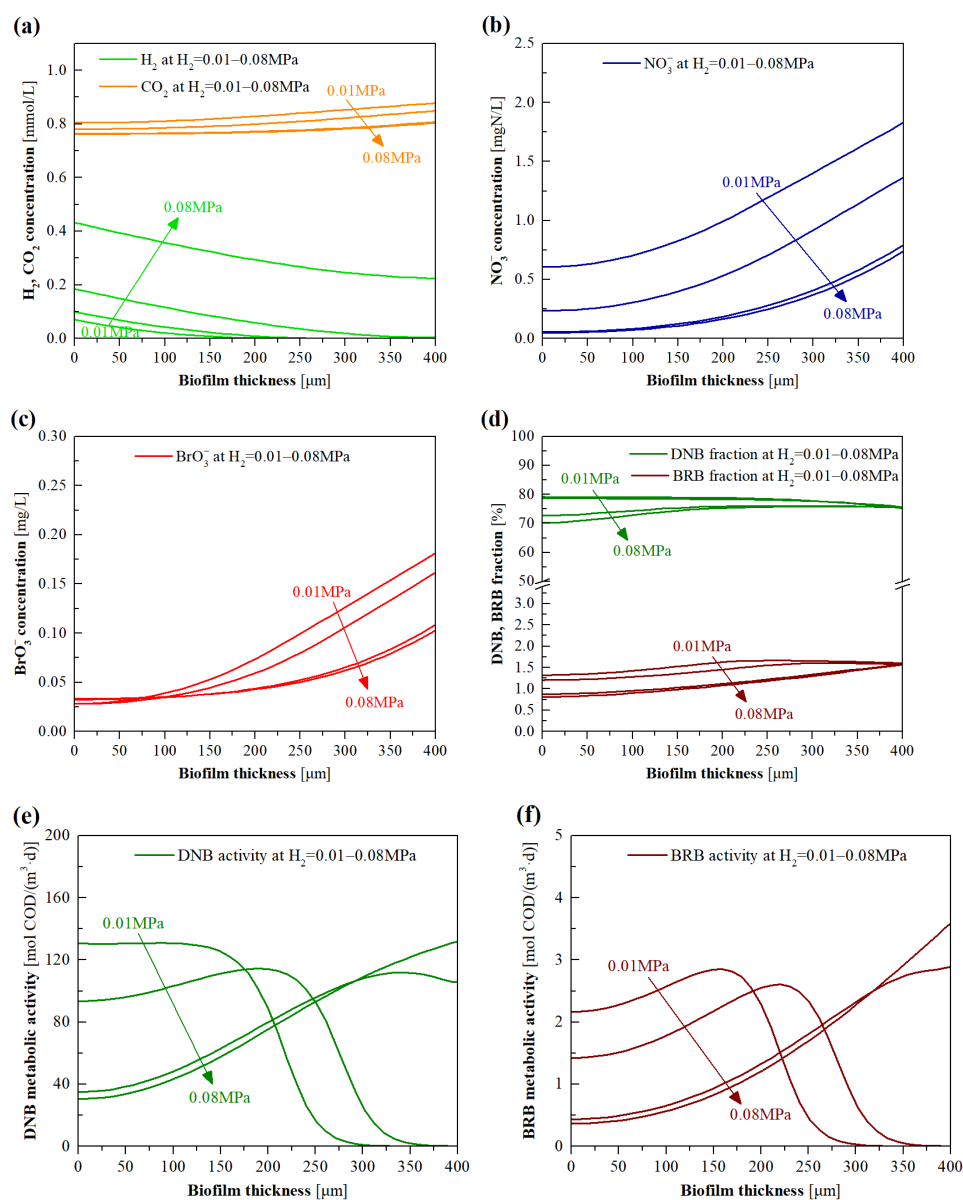


Figure 8. Model simulated profiles for (a) H₂ and CO₂, (b) NO₃⁻, (c) BrO₃⁻ concentrations, and (d) DNB and BRB fractions, as well as (e) DNB and (f) BRB metabolic activities, in the biofilm of H₂-MBfR as a function of H₂ pressure ranging from 0.01 to 0.08 MPa.

As depicted in Figure 8b,c, with the increase in H₂ pressure from 0.01 to 0.04 MPa, the NO₃⁻ and BrO₃⁻ concentrations in the biofilm were found to markedly decline. This can be explained by the increased H₂ availability for DNB and BRB compared to the biofilm exterior, which allowed a greater reduction in NO₃⁻ and BrO₃⁻ in the exterior rather than the interior of biofilm. However, NO₃⁻ and BrO₃⁻ concentration gradients hardly varied once the H₂ pressure exceeded 0.04 MPa, which is in accordance with the experimental findings of the short-term experiments that the NO₃⁻ and BrO₃⁻ removal marginally changed at the excessive H₂ pressure (shown in Figure 6b). According to the simulated BrO₃⁻ concentration profiles, BrO₃⁻ concentrations in the biofilm were all greater than its calibrated half-maximum-rate concentration (0.014 mg/L) at the simulated H₂ pressure range, indicating that BrO₃⁻ loading was also not a limiting factor to BRB activity. The increased H₂ availability in the outer layer of the biofilm resulted in the extension of the active region of DNB and BRB from the biofilm interior to the whole biofilm, as revealed in Figure 8e,f. In particular, the decreased activities of DNB and BRB in the inner layer of biofilm with increasing H₂ pressure were mainly the consequence of the concurrently

decreased concentrations of NO_3^- and BrO_3^- (Figure 8b,c) and the fractions of DNB and BRB (Figure 8d). In the case of low H_2 pressure (0.01 and 0.02 MPa), the biofilm thicknesses of 200 and 260 μm were the locations where the H_2 concentrations were all below the half-maximum-rate concentrations of DNB and BRB (Figure 8a); beyond these thicknesses, the metabolic activities of DNB and BRB began to dramatically decrease, as delineated in Figure 8e,f.

3.5. Model Evaluation of the Effects of NO_3^- Loading

The experimental results, as shown in Figure 6c, corroborate that the NO_3^- loading significantly impacted the BrO_3^- removal of the H_2 -MBfR. To understand the underlying mechanism, we employed the validated model to simulate the substrate profiles and microbial activities in the biofilm at the influent NO_3^- concentrations of 1–20 mg N/L. As shown in Figure 9a, the H_2 and CO_2 concentration gradients in the biofilm sharply decreased with increasing influent NO_3^- concentration, implying that high NO_3^- loadings might significantly enhance the activity of DNB, leading to greater consumption of these two substrates. In particular, H_2 off-gassing was found at the influent NO_3^- concentration lower than 10 mg N/L, owing to the lack of an electron acceptor for H_2 consumption. Once the influent NO_3^- concentration was greater than 10 mg N/L, NO_3^- was found to accumulate in the biofilm with high concentrations (Figure 9b), presumably due to the limitation of overall DNB population, while over 90% of the inputted BrO_3^- could not be consumed by BRB in the biofilm (Figure 9c), suggesting the severe inhibition of BRB activity by high NO_3^- loadings. As exhibited in Figure 9d, when the influent NO_3^- concentration was increased from 1 to 20 mg N/L, the BRB fractions across the biofilm decreased from beyond 20% to approximately 1%, which was accompanied by the surge of the DNB fraction across the biofilm, suggesting the competitive advantage of DNB over BRB in the case of the high NO_3^- loadings.

Figure 9e,f show the simulated DNB and BRB metabolic activities in the biofilm of the system operated under various influent NO_3^- concentrations. As the influent NO_3^- concentration was less than 10 mg N/L, the high DNB and BRB activities appeared at the outer layer of the biofilm, and a closer distance from the HFM side led to lower activities of DNB and BRB. This trend coincides with that of NO_3^- and BrO_3^- concentration gradients in the biofilm, as shown in Figure 9b,c. When the influent NO_3^- concentration was higher than 10 mg N/L, the DNB activities sharply dropped at the biofilm thickness of beyond 210 μm . This is because the H_2 concentrations in the locations beyond this thickness were lower than the half-maximum-rate concentration of DNB (0.002 mg/L). In addition, the BRB activities were strongly inhibited at the higher influent NO_3^- concentration (especially 20 mg N/L), indicating that BRB was overwhelmed by DNB for electron donor competition, when NO_3^- concentration in the influent was much higher than that of BrO_3^- . This is consistent with the previous findings that an excessive influent NO_3^- concentration could inhibit BrO_3^- reduction [6,30].

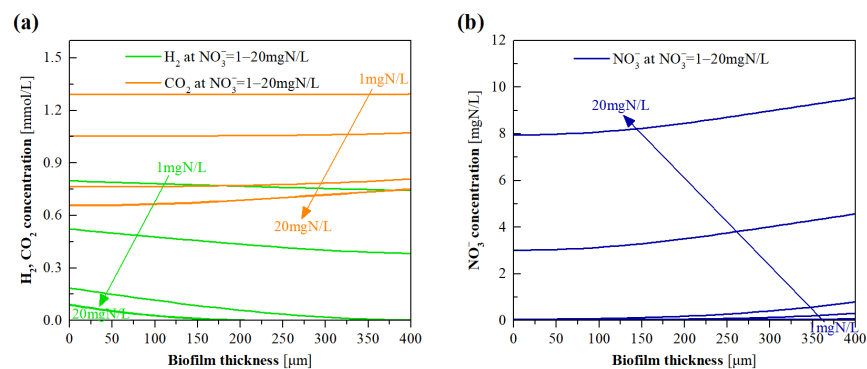


Figure 9. Cont.

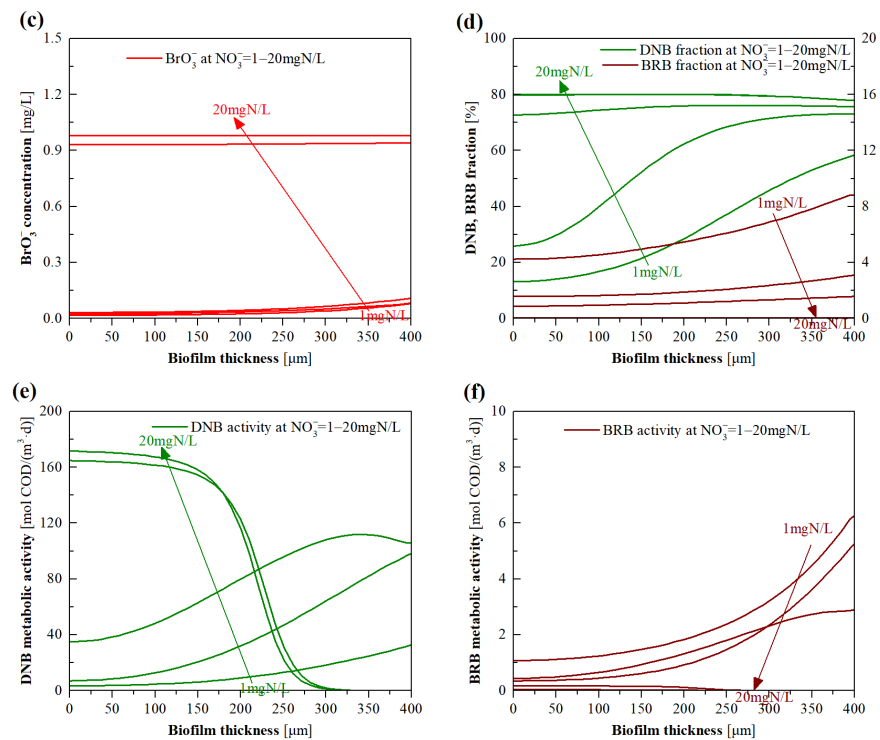


Figure 9. Model simulated profiles for (a) H₂ and CO₂, (b) NO₃⁻, (c) BrO₃⁻ concentrations, and (d) DNB and BRB fractions, as well as (e) DNB and (f) BRB metabolic activities, in the biofilm of H₂-MBfR as a function of influent NO₃⁻ concentration ranging from 1 to 20 mg/N/L.

3.6. Model Evaluation of the Effects of CO₂ Pressure

CO₂ has dual functions, i.e., as a carbon source to support microorganism growth and for pH control to regulate the microbial activities in H₂-MBfRs [19,31]. Simulations were, therefore, conducted to investigate the effects of CO₂ addition on the evolution of stratification characteristics of the biofilm at the supply pressure of 0.004–0.036 MPa. As shown in Figure 10a–c, the increase in CO₂ pressure from 0.004 to 0.02 MPa led to insignificant changes in the H₂, NO₃⁻, and BrO₃⁻ concentration gradients of the biofilm. Once the CO₂ pressure was higher than 0.02 MPa, the accumulation of H₂ and NO₃⁻ was increased in the biofilm. The BrO₃⁻ concentrations in the biofilm were slightly increased at the CO₂ pressure of 0.036 MPa. This implies that DNB was more sensitive to the acidic conditions (pH 6.0–6.2 at CO₂ pressure 0.028–0.036 MPa) than BRB.

As depicted in Figure 10d, as the CO₂ pressure was increased from 0.004 to 0.036 MPa, no apparent difference was found in the DNB fractions, while a slight increase in the BRB fractions was observed. It can be seen from Figure 10e,f that, when the CO₂ pressure was less than 0.02 MPa, the DNB and BRB activities in the biofilm all gradually augmented with the increase in distance from the HFM side. This can be attributed to the relatively higher NO₃⁻ and BrO₃⁻ concentrations in the biofilm exterior. It is interesting to note that, compared to the activities of DNB and BRB at the CO₂ pressure below 0.02 MPa, a CO₂ pressure beyond this value gave rise to decreased and increased microbial activities in the exterior and interior of the biofilm, respectively. This can be explained by the fact that DNB and BRB in the biofilm exterior were in the vicinity of the bulk liquid, and the acidification of bulk liquid severely inhibited their metabolic activities; subsequently, the declined activities of microorganisms in the biofilm exterior led to more diffusion of NO₃⁻ and BrO₃⁻ toward the HFM side (Figure 10b,c), which consequently led to increased activities of DNB and BRB in the biofilm interior. When the CO₂ pressure was increased from 0.012 to 0.036 MPa, DNB activity in the majority of the biofilm significantly declined, while the decreased BRB activity in the biofilm exterior was accompanied by an increase in

BRB activity in the biofilm interior (Figure 10e,f). This also indicates that BRB was more tolerant of the acidic aquatic environment than DNB.

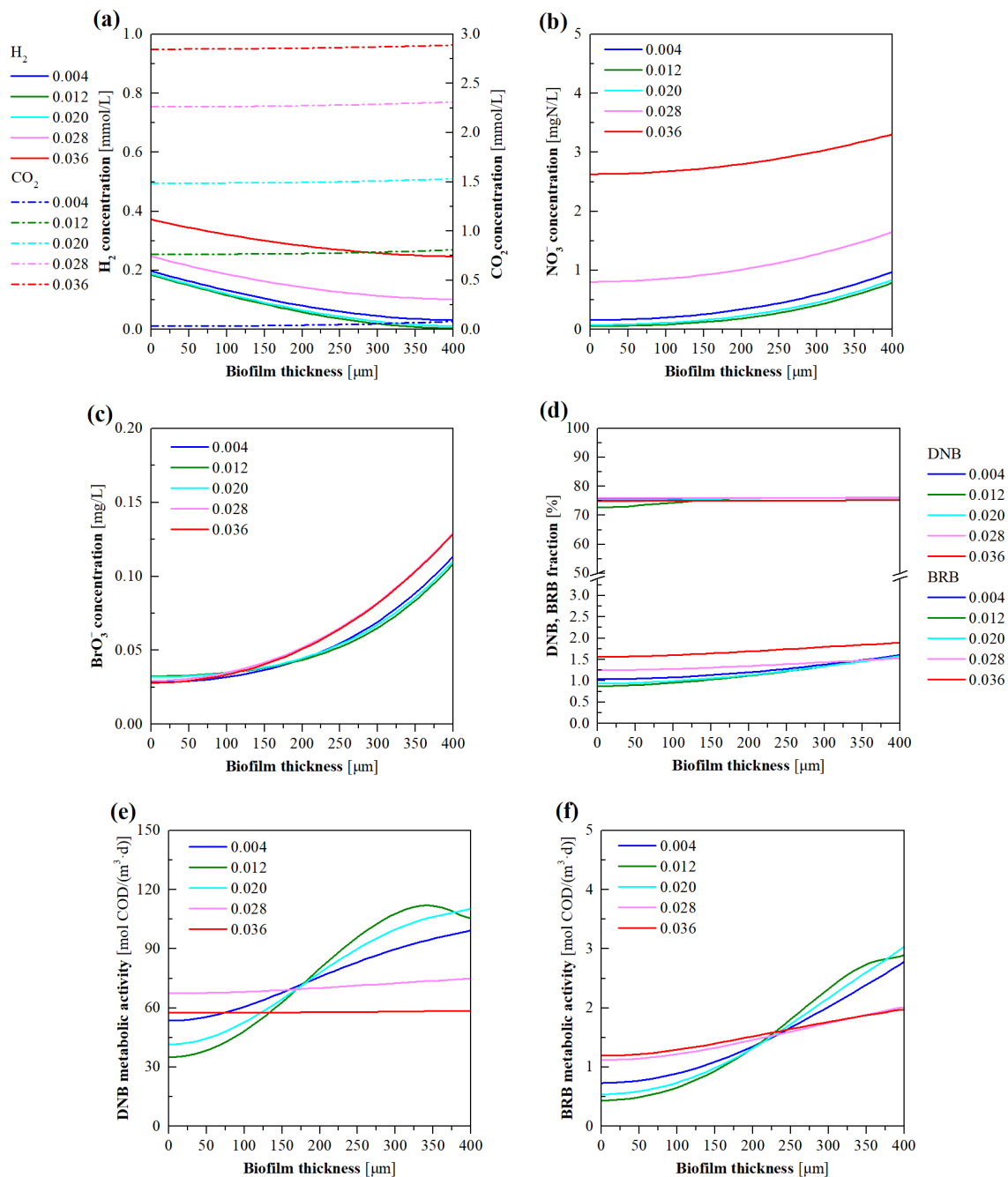


Figure 10. Model simulated profiles for (a) H₂ and CO₂, (b) NO₃⁻, (c) BrO₃⁻ concentrations, and (d) DNB and BRB fractions, as well as (e) DNB and (f) BRB metabolic activities, in the biofilm of H₂-MBfR as a function of CO₂ pressure ranging from 0.004 to 0.036 MPa.

4. Conclusions

An expanded multispecies model was developed to provide key information regarding the microbial BrO₃⁻ and NO₃⁻ reduction processes in the H₂-MBfR in diverse operating conditions. The selected model parameters, K_m , μ_{BRB} , μ_{DNB} , and K_{BrO_3} , were calibrated to the best-fit values of 0.189 m/day, 0.85 day⁻¹, 0.57 day⁻¹, and 0.014 mg/L, respectively. The good agreement between experimental measurements and modeled results indicates the accuracy and reliability of the calibrated model. The evolution of the substrate gradients, as

well as microbial fraction and activity, was driven by the changing system operating parameters involving H_2 pressure, BrO_3^- and NO_3^- loading, and CO_2 pressure. Increasing H_2 pressure led to more efficient BrO_3^- and NO_3^- reduction in the biofilm, but an exorbitant pressure (beyond 0.04 MPa) gave rise to off-gassing of H_2 . The augment in BrO_3^- loading had no significant influence on NO_3^- reduction, while an influent NO_3^- concentration higher than 10 mg N/L resulted in the apparent inhibition of BrO_3^- reduction. A CO_2 pressure over 0.02 MPa had a distinct negative influence on NO_3^- reduction, but minorly impacted BrO_3^- reduction. The simulation results of the developed model offer important mechanistic insights into the BrO_3^- and NO_3^- reduction processes of H_2 -MBfR.

Supplementary Materials: The following supporting information can be downloaded at <https://www.mdpi.com/article/10.3390/membranes12080774/s1>: Table S1. Short-term operational conditions of influencing factor experiment of the H_2 -MBfR; Table S2. Start-up and long-term operational conditions of the H_2 -MBfR; Table S3. Stoichiometric and kinetic parameters of BRB related metabolic process for the developed model; Table S4. Experiments operational parameters for the model development; Table S5. Other pertinent input parameters for model development; Section S1. Calculation of the stoichiometric coefficients for BRB metabolic process. Refs. [32,33] are cited on Supplementary Materials.

Author Contributions: Conceptualization, J.Z. (Junjian Zheng), M.J. and H.L.; methodology, M.J. and J.Z. (Junjian Zheng); software, M.J.; validation, Y.Z., J.Z. (Jie Zhang), X.Z. and Z.W.; formal analysis, Y.Z. and X.D.; investigation, Y.Z. and X.D.; resources, J.Z. (Junjian Zheng), H.L., X.Z. and Z.W.; data curation, M.J. and Y.Z.; writing—original draft preparation, M.J.; writing—review and editing, J.Z. (Junjian Zheng); visualization, J.Z. (Junjian Zheng) and J.Z. (Jie Zhang); supervision, X.Z. and Z.W.; project administration, J.Z. (Junjian Zheng); funding acquisition, J.Z. (Junjian Zheng), M.J., Y.Z. and H.L. All authors have read and agreed to the published version of the manuscript.

Funding: This research was funded by the Guangxi Natural Science Foundation (grant number 2022GXNSFFA035033), the National Natural Science Foundation of China (grant numbers 52000046, 52100034, and 51878197), the Special Project of Guangxi Science and Technology Base and Talent (grant numbers GuiKe AD20297009 and GuiKe AD20297007), and the Middle-aged and Young Teachers' Basic Ability Promotion Project of Guangxi (grant numbers 2022KY0179, 2021KY0221, and 2020KY05039).

Institutional Review Board Statement: Not applicable.

Data Availability Statement: Not applicable.

Conflicts of Interest: The authors declare no conflict of interest.

References

1. Martin, K.J.; Downing, L.S.; Nerenberg, R. Evidence of specialized bromate-reducing bacteria in a hollow fiber membrane biofilm reactor. *Water Supply* **2009**, *8*, 473–479. [[CrossRef](#)]
2. Xiao, Q.; Yu, S. Reduction of bromate from drinking water by sulfite/ferric ion systems: Efficacy and mechanisms. *J. Hazard. Mater.* **2021**, *418*, 125940. [[CrossRef](#)] [[PubMed](#)]
3. Yang, J.; Dong, Z.; Jiang, C.; Wang, C.; Liu, H. An overview of bromate formation in chemical oxidation processes: Occurrence, mechanism, influencing factors, risk assessment, and control strategies. *Chemosphere* **2019**, *237*, 124521. [[CrossRef](#)] [[PubMed](#)]
4. Butler, R.; Ehrenberg, S.; Godley, A.R.; Lake, R.; Lytton, L.; Cartmell, E. Remediation of bromate-contaminated groundwater in an ex situ fixed-film bioreactor. *Sci. Total Environ.* **2006**, *366*, 12–20. [[CrossRef](#)]
5. Jahan, B.N.; Li, L.; Pagilla, K.R. Fate and reduction of bromate formed in advanced water treatment ozonation systems: A critical review. *Chemosphere* **2021**, *266*, 128964. [[CrossRef](#)]
6. Zhong, Y.; Yang, Q.; Fu, G.; Xu, Y.; Cheng, Y.; Chen, C.; Xiang, R.; Wen, T.; Li, X.; Zeng, G. Denitrifying microbial community with the ability to bromate reduction in a rotating biofilm-electrode reactor. *J. Hazard. Mater.* **2018**, *342*, 150–157. [[CrossRef](#)]
7. Zhou, W.; Yang, Y.; Gai, W.-Z.; Deng, Z.-Y. A comparative study on high-efficient reduction of bromate in neutral solution using zero-valent Al treated by different procedures. *Sci. Total Environ.* **2021**, *795*, 148786. [[CrossRef](#)]
8. Xia, S.; Liang, J.; Xu, X.; Shen, S. Simultaneous removal of selected oxidized contaminants in groundwater using a continuously stirred hydrogen-based membrane biofilm reactor. *J. Environ. Eng.* **2013**, *25*, 96–104. [[CrossRef](#)]
9. Chen, X.; Liu, Y.; Peng, L.; Ni, B.-J. Perchlorate, nitrate, and sulfate reduction in hydrogen-based membrane biofilm reactor: Model-based evaluation. *Chem. Eng. J.* **2017**, *316*, 82–90. [[CrossRef](#)]

10. Jiang, M.; Zhang, Y.; Yuan, Y.; Chen, Y.; Lin, H.; Zheng, J.; Li, H.; Zhang, X. Nitrate removal and dynamics of microbial community of a hydrogen-based membrane biofilm reactor at diverse nitrate loadings and distances from hydrogen supply end. *Water* **2020**, *12*, 3196. [[CrossRef](#)]
11. Lai, C.-Y.; Lv, P.-L.; Dong, Q.-Y.; Yeo, S.L.; Rittmann, B.E.; Zhao, H.-P. Bromate and nitrate bioreduction coupled with poly-beta-hydroxybutyrate production in a methane-based membrane biofilm reactor. *Environ. Sci. Technol.* **2018**, *52*, 7024–7031. [[CrossRef](#)] [[PubMed](#)]
12. Martin, K.J.; Picioreanu, C.; Nerenberg, R. Assessing microbial competition in a hydrogen-based membrane biofilm reactor (MBfR) using multidimensional modeling. *Biotechnol. Bioeng.* **2015**, *112*, 1843–1853. [[CrossRef](#)] [[PubMed](#)]
13. Jiang, M.; Zheng, J.; Perez-Calleja, P.; Picioreanu, C.; Lin, H.; Zhang, X.; Zhang, Y.; Li, H.; Nerenberg, R. New insight into CO₂-mediated denitrification process in H₂-based membrane biofilm reactor: An experimental and modeling study. *Water Res.* **2020**, *184*, 116177. [[CrossRef](#)] [[PubMed](#)]
14. Tang, Y.; Zhao, H.; Marcus, A.K.; Krajmalnik-Brown, R.; Rittmann, B.E. A steady-state biofilm model for simultaneous reduction of nitrate and perchlorate, part 1: Model development and numerical solution. *Environ. Sci. Technol.* **2012**, *46*, 1598–1607. [[CrossRef](#)]
15. Downing, L.S.; Nerenberg, R. Kinetics of microbial bromate reduction in a hydrogen-oxidizing, denitrifying biofilm reactor. *Biotechnol. Bioeng.* **2007**, *98*, 543–550. [[CrossRef](#)]
16. Tang, Y.; Zhao, H.; Marcus, A.K.; Krajmalnik-Brown, R.; Rittmann, B.E. A steady-state biofilm model for simultaneous reduction of nitrate and perchlorate, part 2: Parameter optimization and results and discussion. *Environ. Sci. Technol.* **2012**, *46*, 1608–1615. [[CrossRef](#)]
17. Li, H.; Zhou, L.; Lin, H.; Zhang, W.; Xia, S. Nitrate Effects on Perchlorate Reduction in a H₂/CO₂-based Biofilm. *Sci. Total Environ.* **2019**, *694*, 133564. [[CrossRef](#)]
18. Lee, K.-C.; Rittmann, B.E. Applying a novel autohydrogenotrophic hollow-fiber membrane biofilm reactor for denitrification of drinking water. *Water Res.* **2002**, *36*, 2040–2052. [[CrossRef](#)]
19. Tang, Y.; Zhou, C.; Ziv-El, M.; Rittmann, B.E. A pH-control model for heterotrophic and hydrogen-based autotrophic denitrification. *Water Res.* **2011**, *45*, 232–240. [[CrossRef](#)]
20. Wu, J.; Yin, Y.; Wang, J. Hydrogen-based membrane biofilm reactors for nitrate removal from water and wastewater. *Int. J. Hydrogen Energ.* **2018**, *43*, 1–15. [[CrossRef](#)]
21. Estuardo, C.; Martí, M.C.; Huiliñir, C.; Aspé Lillo, E.; Roeckel von Bennewitz, M. Improvement of nitrate and nitrite reduction rates prediction. *Electron. J. Biotechnol.* **2008**, *11*, 73–82. [[CrossRef](#)]
22. Vavilin, V.A.; Vasiliev, V.B.; Rytov, S.V.; Ponomarev, A.V. Self-oscillating coexistence of methanogens and sulfate-reducers under hydrogen sulfide inhibition and the pH-regulating effect. *Bioresour. Technol.* **1994**, *49*, 105–119. [[CrossRef](#)]
23. Angelidaki, I.; Ellegaard, L.; Ahring, B.K. A mathematical model for dynamic simulation of anaerobic digestion of complex substrates: Focusing on ammonia inhibition. *Biotechnol. Bioeng.* **1993**, *42*, 159–166. [[CrossRef](#)] [[PubMed](#)]
24. Jiang, M.; Zhang, Y.; Zheng, J.; Li, H.; Ma, J.; Zhang, X.; Wei, Q.; Wang, X.; Zhang, X.; Wang, Z. Mechanistic insights into CO₂ pressure regulating microbial competition in a hydrogen-based membrane biofilm reactor for denitrification. *Chemosphere* **2022**, *303*, 134875. [[CrossRef](#)] [[PubMed](#)]
25. Tang, Y.; Ontiveros-Valencia, A.; Feng, L.; Zhou, C.; Krajmalnik-Brown, R.; Rittmann, B.E. A biofilm model to understand the onset of sulfate reduction in denitrifying membrane biofilm reactors. *Biotechnol. Bioeng.* **2013**, *110*, 763–772. [[CrossRef](#)]
26. Lv, X.; Wang, D.; Iqbal, W.; Yang, B.; Mao, Y. Microbial reduction of bromate: Current status and prospects. *Biodegradation* **2019**, *30*, 365–374. [[CrossRef](#)]
27. Pang, S.; Rittmann, B.E.; Wu, C.; Yang, L.; Zhou, J.; Xia, S. Synergistic inorganic carbon and denitrification genes contributed to nitrite accumulation in a hydrogen-based membrane biofilm reactor. *Bioengineering* **2022**, *9*, 222. [[CrossRef](#)]
28. Ghafari, S.; Hasan, M.; Aroua, M.K. Effect of carbon dioxide and bicarbonate as inorganic carbon sources on growth and adaptation of autohydrogenotrophic denitrifying bacteria. *J. Hazard. Mater.* **2009**, *162*, 1507–1513. [[CrossRef](#)]
29. Nerenberg, R. The membrane-biofilm Reactor (MBfR) as a counter-diffusional biofilm process. *Curr. Opin. Biotech.* **2016**, *38*, 131–136. [[CrossRef](#)]
30. Wang, F.; van Halem, D.; Ding, L.; Bai, Y.; Lekkerkerker-Teunissen, K.; van der Hoek, J.P. Effective removal of bromate in nitrate-reducing anoxic zones during managed aquifer recharge for drinking water treatment: Laboratory scale simulations. *Water Res.* **2018**, *130*, 88–97. [[CrossRef](#)]
31. Xia, S.; Xu, X.; Zhou, C.; Wang, C.; Zhou, L.; Rittmann, B.E. Direct Delivery of CO₂ into a Hydrogen-based Membrane Biofilm Reactor and Model Development. *Chem. Eng. J.* **2016**, *290*, 154–160. [[CrossRef](#)]
32. Henze, M.; van Loosdrecht, M.C.; Ekama, G.A.; Brdjanovic, D. *Biological Wastewater Treatment*; IWA Publishing: London, UK, 2008.
33. Lide, D.R. *CRC Handbook of Chemistry and Physics*; CRC: Boca Raton, FL, USA, 2012.